Strongly bound excitons in monolayer PtS_2 and $PtSe_2$

M. Sajjad, N. Singh, and U. Schwingenschlögl

Citation: Appl. Phys. Lett. **112**, 043101 (2018);
View online: https://doi.org/10.1063/1.5010881
View Table of Contents: http://aip.scitation.org/toc/apl/112/4
Published by the American Institute of Physics

Strongly bound excitons in monolayer PtS_2 and $PtSe_2$

M. Sajjad, N. Singh, and U. Schwingenschlögl[a)]
King Abdullah University of Science and Technology (KAUST), Physical Science and Engineering Division (PSE), Thuwal 23955-6900, Saudi Arabia

(Received 27 October 2017; accepted 2 January 2018; published online 22 January 2018)

Based on first-principles calculations, the structural, electronic, and optical properties of monolayers PtS_2 and $PtSe_2$ are investigated. The bond stiffnesses and elastic moduli are determined by means of the spring constants and strain-energy relations, respectively. Dynamic stability is confirmed by calculating the phonon spectra, which shows excellent agreement with experimental reports for the frequencies of the Raman-active modes. The Heyd-Scuseria-Ernzerhof functional results in electronic bandgaps of 2.66 eV for monolayer PtS_2 and 1.74 eV for monolayer $PtSe_2$. G_0W_0 calculations combined with the Bethe-Salpeter equation are used to predict the optical spectra and exciton binding energies (0.78 eV for monolayer PtS_2 and 0.60 eV for monolayer $PtSe_2$). It turns out that the excitons are strongly bound and therefore very stable against external perturbations. *Published by AIP Publishing*. https://doi.org/10.1063/1.5010881

The zero bandgap nature of famous graphene has triggered a lot of interest in semiconducting two-dimensional materials, including boron nitride,[1] transition metal dichalcogenides (TMDCs),[2–12] transition-metal trichalcogenides,[13,14] and phosphorene.[15–19] In bulk TMDCs, covalently bound TM and chalcogen atoms form layers held together by weak van der Waals forces, which opens access to a rich class of two-dimensional materials with considerable bandgaps of 1–2 eV and potential applications in field-effect transistors,[20–23] logic circuits,[24] and memory devices,[25] for example. To date, mainly 2H phase monolayer TMDCs have been used, fabricated by exfoliation or chemical vapor deposition, while 1T phase monolayer TMDCs received attention only recently.

Despite the high cost of Pt, 1T phase Pt dichalcogenides are interesting because of their high carrier mobilities[26] (as compared to the Mo and W dichalcogenides[23,27,28]) combined with the possibility to tune the bandgap by the film thickness,[29] which is beneficial for constructing functional devices. Monolayer $PtSe_2$, synthesized by direct selenization of a Pt(111) substrate,[30] is known to be stable in air with high photo-responsivity[26] and can be used to sense NO_2 with ultrahigh sensitivity and fast response time.[31] In addition, the unconventional R-2 Rashba effect has been realized for the first time in monolayer $PtSe_2$.[32] Strong interlayer interactions and bandgaps of 1.6 eV (Ref. 29) and 1.2 eV (Ref. 30) have been reported for monolayers PtS_2 and $PtSe_2$, respectively, which is the spectral range of interest for solar energy harvesting. However, the optical properties of Pt dichalcogenides are hardly investigated, in contrast to the 2H phase monolayer TMDCs.[6,10,11] To overcome this knowledge gap, we employ in the present work first-principles calculations and the Bethe-Salpeter equation (BSE) to predict the absorption spectra and exciton binding energies of monolayers PtS_2 and $PtSe_2$. The bond stiffnesses, elastic moduli, phonon spectra, and electronic band structures of the two materials are calculated and analyzed.

We employ density functional theory using the projector augmented plane wave method as implemented in the Vienna *Ab-initio* Simulation Package.[33] Monolayer structures are constructed by taking one chalcogen-Pt-chalcogen slab from the bulk crystal structures with the experimental lattice constants[29,34] and complementing it with a vacuum layer thicker than 16 Å in the out-of-plane direction (which also prevents artifacts of the periodic boundary conditions). The van der Waals correction of Grimme is employed,[35] and the spin-orbit coupling is taken into account (except for the structure relaxation and BSE calculations) because Pt is a heavy element. The lattice constants and atomic positions are relaxed using the Perdew-Burke-Ernzerhof (PBE) generalized gradient approximation (plane wave cutoff energy of 450 eV, $6 \times 6 \times 1$ k-mesh) until the energy is converged within 10 meV and the atomic forces have dropped below 1 meV/Å. Heyd-Scuseria-Ernzerhof (HSE06) calculations are performed starting from the converged PBE wave functions (plane wave cutoff energy of 450 eV, $8 \times 8 \times 1$ k-mesh). G_0W_0 calculations to obtain the quasi-particle energies are then conducted based on the HSE06 single-particle energies and wave functions ($8 \times 8 \times 1$ k-mesh), using a truncated Coulomb potential. Finally, the BSE optical spectra are derived from the quasi-particle energies, taking into account the 10 highest valence and 10 lowest conduction bands. We construct $5 \times 5 \times 1$ supercells of the monolayer structures to calculate the phonon spectra by means of the second order force constants obtained from density functional perturbation theory,[36] using the PBE functional ($3 \times 3 \times 1$ k-mesh). Strain-energy relations are calculated by changing the lattice constant in steps of 0.5% and relaxing the atomic positions in each step.

As monolayers PtS_2 and $PtSe_2$ belong to the family of 1T phase TMDCs, Pt is octahedrally coordinated by six chalcogen atoms. The side view given in Fig. 1(a) shows that a layer of Pt atoms is sandwiched between layers of chalcogen atoms. The PBE functional overestimates the lattice constants only by 0.5% as compared to the experimental values, see Table I. The spring constants calculated as trace of the

a)udo.schwingenschlogl@kaust.edu.sa. Tel.: +966(0)544700080.

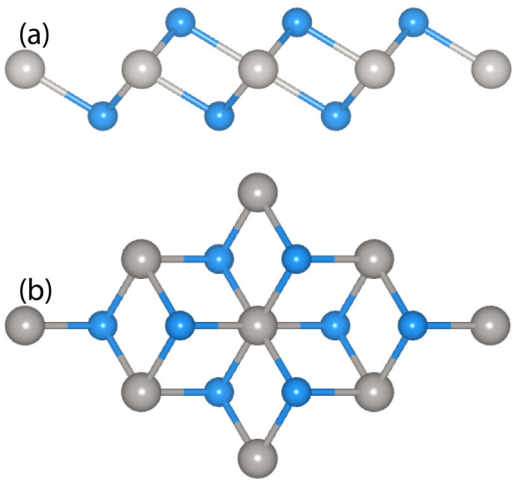

FIG. 1. (a) Side and (b) top views of monolayer PtX_2. The large and small spheres represent the Pt and X atoms, respectively.

TABLE I. Optimized lattice constant, frequencies of the Raman active modes, spring constant, and elastic modulus as obtained by PBE calculations.

	Monolayer PtS_2		Monolayer $PtSe_2$	
	Calculated	Experiment	Calculated	Experiment
a_0 (Å)	3.56	3.54 (Ref. 29)	3.72	3.70 (Ref. 30)
E'' (cm^{-1})	270	302 (Ref. 29)	172	185 (Ref. 26)
A_1' (cm^{-1})	321		212	206 (Ref. 26)
K (eV/Å)	8.8		7.7	
C (N/m)	101		87	

second order force constant tensor (second derivatives of the energy with respect to the displacements of the Pt and chalcogen atoms along the Cartesian axes) are given in Table I. We find that the bond stiffness is smaller for the heavier chalcogen atom, consistent with Ref. 37. The Pt-S and Pt-Se bonds are less stiff than the corresponding bonds in 2H phase monolayers MoS_2 (11.2 eV/Å), $MoSe_2$ (9.8 eV/Å), WS_2 (11.7 eV/Å), and WSe_2 (10.2 eV/Å) but more stiff than those in 1T phase monolayers ZrS_2 (4.6 eV/Å), $ZrSe_2$ (3.7 eV/Å), HfS_2 (5.2 eV/Å), and $HfSe_2$ (4.2 eV/Å).[37] Lower bond stiffness agrees with a reduced span of phonon frequencies (Fig. 2) as compared to the 2H phase monolayer TMDCs reported in Ref. 37. We therefore can also expect lower lattice thermal conductivities for monolayers PtS_2 and $PtSe_2$, which is one of the key requirements for a material with a high thermoelectric figure of merit. The elastic modulus (obtained from the strain-energy relation[38]) is higher for monolayer PtS_2 than for monolayer $PtSe_2$ due to the higher bond stiffness (Table I).

The phonon spectra in Fig. 2 show three acoustic and six optical phonon branches, as the primitive unit cells of monolayers PtS_2 and $PtSe_2$ contain one Pt and two chalcogen atoms. The fact that there are no imaginary frequencies demonstrates the dynamic stability of the two materials. The phonon modes at the Γ point are decomposed as $A_1'(R) + 2A_2''(IR) + 2E_1'(R + IR) + E''(R)$, where R and IR mark Raman and infrared active modes, respectively. The frequencies of the A_1' and E'' modes, given in Table I, show excellent agreement with the experimental values.[26,29] In addition, the frequency of the A_1' mode of monolayer PtS_2 agrees reasonably well with the theoretical value of 338 cm^{-1} reported in Ref. 39. The authors of Ref. 29 have not found the A_1' mode in monolayer PtS_2, most likely due to the limited thickness of their samples. We note that the HSE06 approach is computationally too expensive to perform phonon calculations for the present supercells with 75 atoms. The $3 \times 3 \times 1$ k-mesh used for the phonon calculations is well converged, as the differences to results for a $2 \times 2 \times 1$ k-mesh (Fig. 1 in the supplementary material) are small.

Figure 3 shows the electronic band structures of monolayers PtS_2 and $PtSe_2$ obtained by PBE, HSE06, and G_0W_0 calculations using an $8 \times 8 \times 1$ k-mesh. The corresponding results for a $6 \times 6 \times 1$ k-mesh (Fig. 2 in the supplementary material) exhibit no significant differences; in particular, the values of the bandgap change by less than 0.01 eV. We observe an indirect bandgap nature for both materials. The valence band maximum is located along the Γ-M direction in monolayer PtS_2 and at the Γ point in monolayer $PtSe_2$, while the conduction band minimum appears always along the Γ-M direction. According to Fig. 3, the PBE, HSE06, and G_0W_0 values of the indirect bandgap are 1.76 eV, 2.66 eV, and 3.43 eV for monolayer PtS_2 and 1.18 eV, 1.74 eV, and 2.53 eV for monolayer $PtSe_2$, respectively. Our PBE results thus agree well with Ref. 40 (1.73 eV for

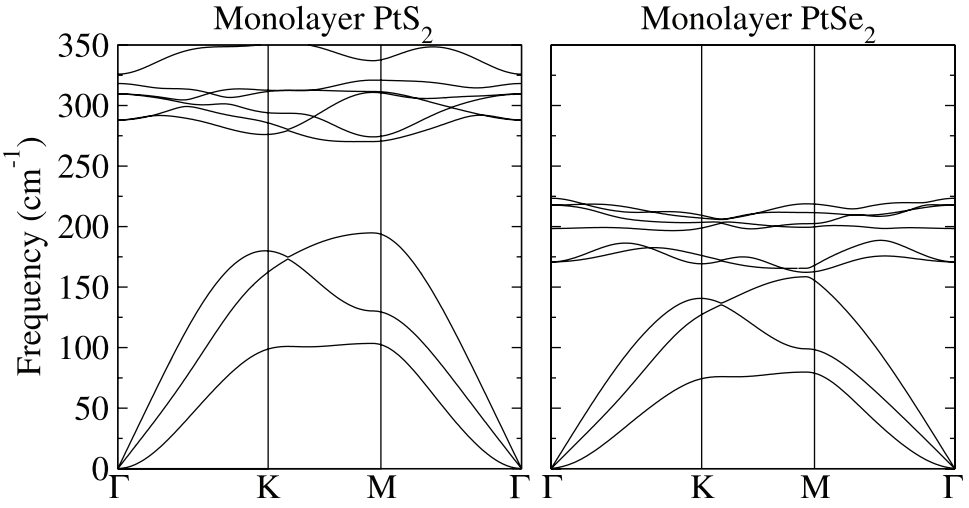

FIG. 2. Phonon band structure as obtained by PBE calculations.

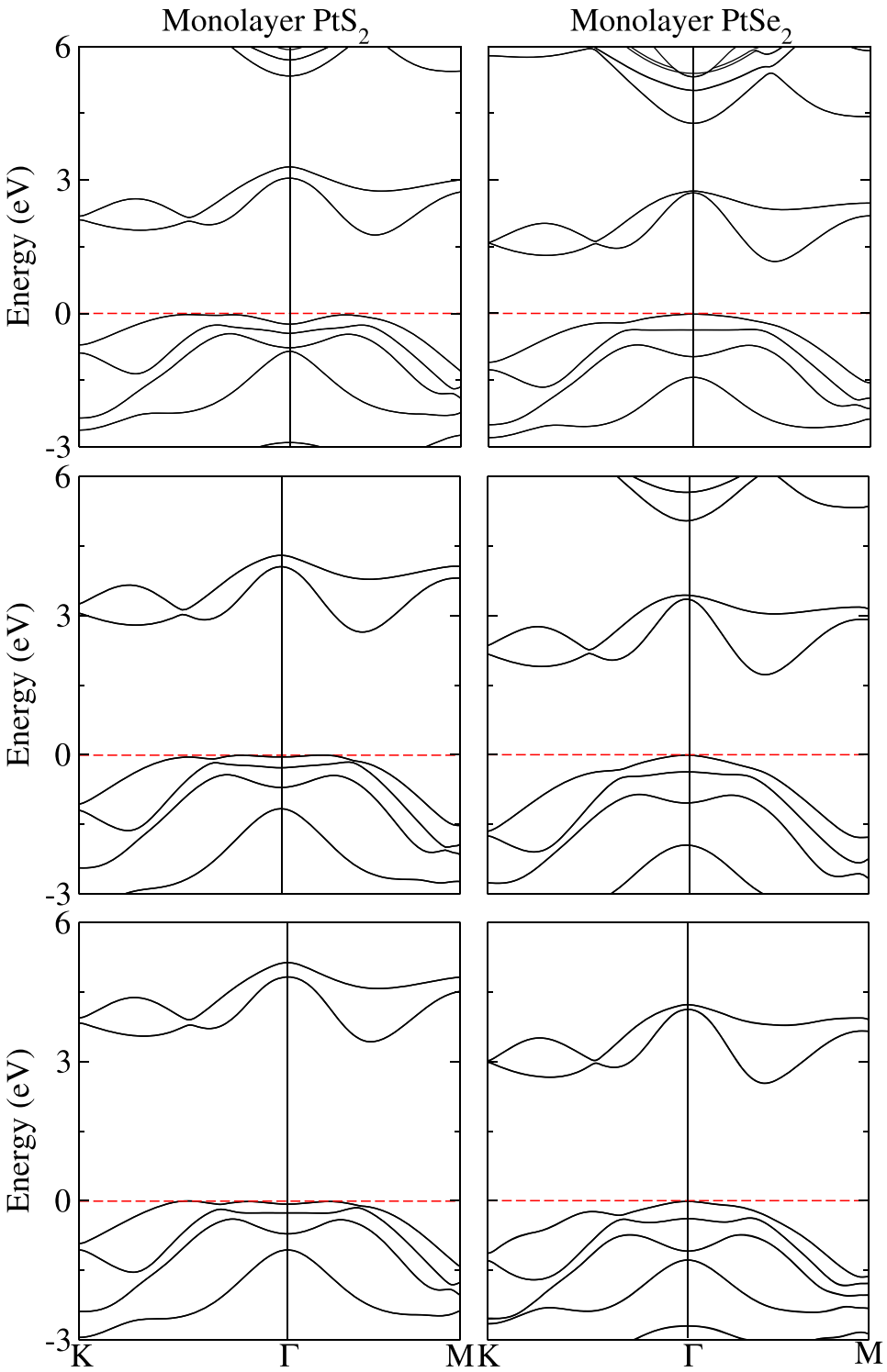

FIG. 3. Electronic band structures as obtained by PBE (top), HSE06 (middle), and G_0W_0 (bottom) calculations using an $8 \times 8 \times 1$ k-mesh.

monolayer PtS_2 and 1.20 eV for monolayer $PtSe_2$). When we calculate the G_0W_0 values based on the PBE single-particle energies and wave functions, we obtain 2.88 eV and 2.06 eV for monolayers PtS_2 and $PtSe_2$, respectively, which agrees for both materials with Ref. 41 (2.83 eV and 2.10 eV) but only for monolayer PtS_2 with Ref. 42 (2.95 eV and 2.48 eV). The partial densities of states given in Fig. 4 demonstrate that the valence and conduction band edges of monolayers PtS_2 and $PtSe_2$ are due to hybridized Pt *d* and chalcogen *p* states.

As the electron-hole interaction is crucial for the absorption behavior of two-dimensional semiconductors, we calculate the optical spectra of monolayers PtS_2 and $PtSe_2$ by the G_0W_0/BSE scheme. Similar to monolayer MoS_2, excitonic peaks appear in Fig. 5 below the minimal direct bandgap. The corresponding results in the random phase approximation (HSE06 functional) show no features in this energy range. The difference between the minimal direct bandgap (G_0W_0) and the energy of an excitonic peak in the optical spectrum is the exciton binding energy. In the case of an $18 \times 18 \times 1$ ($14 \times 14 \times 1$) k-mesh, the first excitonic peak appears at 2.74 eV (2.77 eV) for monolayer PtS_2 and at 2.22 eV (2.23 eV) for monolayer $PtSe_2$. Minimal direct bandgaps of 3.54 eV (3.52 eV) and 2.81 eV (2.82 eV) thus

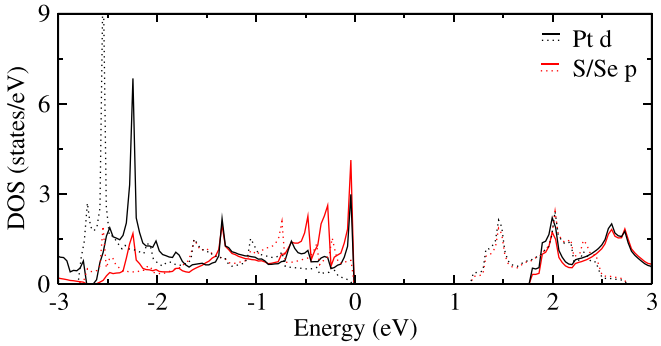

FIG. 4. Partial densities of states of monolayer PtS_2 (solid) and monolayer $PtSe_2$ (dotted) as obtained by PBE calculations.

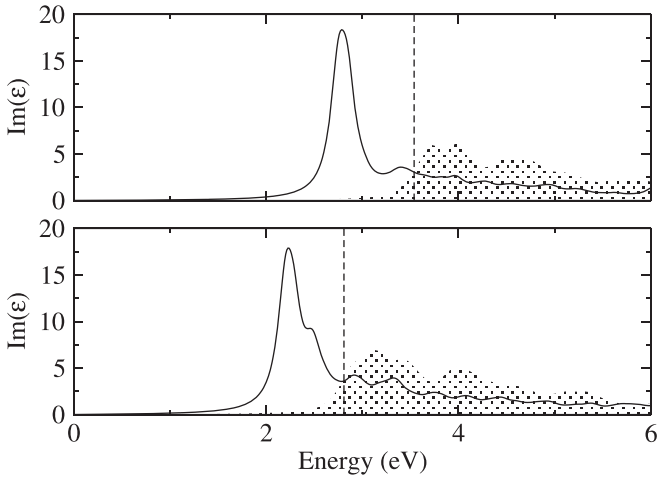

FIG. 5. Imaginary part of the dielectric function as obtained by the G_0W_0/BSE scheme. The corresponding results in the random phase approximation (HSE06 functional) are displayed as gray shades. Vertical lines mark the minimal direct bandgaps according to the G_0W_0 band structures in Fig. 3.

lead to exciton binding energies of 0.78 eV (0.77 eV) and 0.60 eV (0.58 eV) for monolayers PtS_2 and $PtSe_2$, respectively. Similarity of the results obtained for the two k-meshes shows that these values are well converged.

Our results agree perfectly with the prediction of the Mott-Wannier model of two-dimensional materials that (in the case of high polarizability) the exciton binding energy is inversely proportional to the polarizability (ratio of obtained exciton binding energies: $0.78/0.60 = 1.3$; inverse ratio of polarizabilities: $50.2/38.7 = 1.3$).[43] Interestingly, the exciton binding energies of the materials under investigation are much higher than those predicted for 1T phase monolayer SnS_2 [0.41 eV (Ref. 44)] This is a significant finding because strongly bound excitons give rise to stable material properties. In addition, the excitons can sustain strong electric fields and high carrier injection. It turns out that the application of 2% tensile strain red-shifts the first excitonic peak to 2.49 eV for monolayer PtS_2 and to 1.98 eV for monolayer $PtSe_2$. Minimal direct bandgaps of 3.24 eV and 2.52 eV then result in exciton binding energies of 0.75 eV and 0.55 eV for monolayers PtS_2 and $PtSe_2$, respectively.

In conclusion, we have demonstrated the absence of negative phonon frequencies and therefore the dynamic stability of the two-dimensional structures for monolayers PtS_2 and $PtSe_2$. The frequencies of the Raman active modes show excellent agreement with experimental reports. The bond stiffness is found to be lower than those in monolayers MoS_2, $MoSe_2$, WS_2, and WSe_2. We observe indirect bandgaps and hybridization between the Pt *d* and chalcogen *p* states at the valence and conduction band edges. The lowest energy optical transitions turn out to be due to strongly bound excitons, which is of great interest from an application point of view.

See supplementary material for two figures: Phonon band structure as obtained by PBE calculations using a $2 \times 2 \times 1$ k-mesh; Electronic band structures as obtained by PBE, HSE06, and G_0W_0 calculations using a $6 \times 6 \times 1$ k-mesh.

The research reported in this publication was supported by funding from the King Abdullah University of Science and Technology (KAUST).

[1]D. Pacile, J. C. Meyer, C. O. Girit, and A. Zettl, "The two-dimensional phase of boron nitride: Few-atomic-layer sheets and suspended membranes," Appl. Phys. Lett. **92**, 133107 (2008).
[2]H. S. S. R. Matte, A. Gomathi, A. K. Manna, D. J. Late, R. Datta, S. K. Pati, and C. N. R. Rao, "MoS_2 and WS_2 analogues of graphene," Angew. Chem., Int. Ed. **49**, 4059–4062 (2010).
[3]J. N. Coleman, M. Lotya, A. O'Neill, S. D. Bergin, P. J. King, U. Khan, K. Young, A. Gaucher, S. De, R. J. Smith, I. V. Shvets, S. K. Arora, G. Stanton, H.-Y. Kim, K. Lee, G. T. Kim, G. S. Duesberg, T. Hallam, J. J. Boland, J. J. Wang, J. F. Donegan, J. C. Grunlan, G. Moriarty, A. Shmeliov, R. J. Nicholls, J. M. Perkins, E. M. Grieveson, K. Theuwissen, D. W. McComb, P. D. Nellist, and V. Nicolosi, "Two-dimensional nanosheets produced by liquid exfoliation of layered materials," Science **331**, 568–571 (2011).
[4]Q. H. Wang, K. Kalantar-Zadeh, A. Kis, J. N. Coleman, and M. S. Strano, "Electronics and optoelectronics of two-dimensional transition metal dichalcogenides," Nat. Nanotechnol. **7**, 699–712 (2012).
[5]J. Feng, L. Peng, C. Wu, X. Sun, S. Hu, C. Lin, J. Dai, J. Yang, and Y. Xie, "Giant moisture responsiveness of VS_2 ultrathin nanosheets for novel touchless positioning interface," Adv. Mater. **24**, 1969–1974 (2012).
[6]A. Ramasubramaniam, "Large excitonic effects in monolayers of molybdenum and tungsten dichalcogenides," Phys. Rev. B **86**, 115409 (2012).
[7]H. Shi, H. Pan, Y.-W. Zhang, and B. I. Yakobson, "Tuning magnetism of monolayer MoS_2 by doping vacancy and applying strain," Phys. Rev. B **87**, 155304 (2013).
[8]D. Y. Qiu, F. H. da Jornada, and S. G. Louie, "Optical spectrum of MoS_2: Many-body effects and diversity of exciton states," Phys. Rev. Lett. **111**, 216805 (2013).
[9]Y. Liang, S. Huang, R. Soklaski, and L. Yang, "Quasiparticle band-edge energy and band offsets of monolayer of molybdenum and tungsten chalcogenide," Appl. Phys. Lett. **103**, 042106 (2013).
[10]M. M. Ugeda, A. J. Bradley, S.-F. Shi, F. H. da Jornada, Y. Zhang, D. Y. Qiu, W. Ruan, S.-K. Mo, Z. Hussain, Z.-X. Shen, F. Wang, S. G. Louie, and M. F. Crommie, "Giant bandgap renormalization and excitonic effects in a monolayer transition metal dichalcogenide semiconductor," Nat. Mater. **13**, 1091–1095 (2014).
[11]A. T. Hanbicki, M. Currie, G. Kioseoglou, A. L. Friedman, and B. T. Jonker, "Measurement of high exciton binding energy in the monolayer transition-metal dichalcogenides WS_2 and WSe_2," Solid State Commun. **203**, 16–20 (2015).
[12]P. J. Jeon, S. Min, J. S. Kim, S. R. A. Raza, K. Choi, H. S. Lee, Y. T. Lee, D. K. Hwang, H. J. Choi, and S. Im, "Enhanced device performances of WSe_2-MoS_2 van der Waals junction p-n diode by fluoropolymer encapsulation," J. Mater. Chem. C **3**, 2751–2758 (2015).
[13]J. Dai and X. C. Zeng, "Titanium trisulfide monolayer: Theoretical prediction of a new direct-gap semiconductor with high and anisotropic carrier mobility," Angew. Chem., Int. Ed. **54**, 7572–7576 (2015).
[14]M. Li, J. Dai, and X. C. Zeng, "Tuning the electronic properties of transition-metal trichalcogenides via tensile strain," Nanoscale **7**, 15385–15391 (2015).

[15]L. Li, Y. Yu, G. J. Ye, Q. Ge, X. Ou, H. Wu, D. Feng, X. H. Chen, and Y. Zhang, "Black phosphorus field-effect transistors," Nat. Nanotechnol. **9**, 372–377 (2014).
[16]J. Dai and X. C. Zeng, "Bilayer phosphorene: Effect of stacking order on bandgap and its potential applications in thin-film solar cells," J. Phys. Chem. Lett. **5**, 1289–1293 (2014).
[17]H. Guo, N. Lu, J. Dai, X. J. Wu, and X. C. Zeng, "Phosphorene nanoribbons, phosphorus nanotubes, and van der Waals multilayers," J. Phys. Chem. C **118**, 14051–14059 (2014).
[18]Y. H. Xu, J. Dai, and X. C. Zeng, "Electron-transport properties of few-layer black phosphorus," J. Phys. Chem. Lett. **6**, 1996–2002 (2015).
[19]M. H. Wu, H. Fu, L. Zhou, K. L. Yao, and X. C. Zeng, "Nine new phosphorene polymorphs with non-honeycomb structures: A much extended family," Nano Lett. **15**, 3557–3562 (2015).
[20]H. Fang, S. Chuang, T. C. Chang, K. Takei, T. Takahashi, and A. Javey, "High-performance single layered WSe_2 p-FETs with chemically doped contacts," Nano Lett. **12**, 3788–3792 (2012).
[21]W. Liu, J. Kang, D. Sarkar, Y. Khatami, D. Jena, and K. Banerjee, "Role of metal contacts in designing high-performance monolayer n-type WSe_2 field effect transistors," Nano Lett. **13**, 1983–1990 (2013).
[22]S. Das, H.-Y. Chen, A. V. Penumatcha, and J. Appenzeller, "High performance multilayer MoS_2 transistors with scandium contacts," Nano Lett. **13**, 100–105 (2013).
[23]H.-J. Chuang, X. Tan, N. J. Ghimire, M. M. Perera, B. Chamlagain, M. M.-C. Cheng, J. Yan, D. Mandrus, D. Tomnek, and Z. Zhou, "High mobility WSe_2 p- and n-type field-effect transistors contacted by highly doped graphene for low-resistance contacts," Nano Lett. **14**, 3594–3601 (2014).
[24]B. Radisavljevic, M. B. Whitwick, and A. Kis, "Integrated circuits and logic operations based on single-layer MoS_2," ACS Nano **5**, 9934–9938 (2011).
[25]S. Bertolazzi, D. Krasnozhon, and A. Kis, "Nonvolatile memory cells based on MoS_2/graphene heterostructures," ACS Nano **7**, 3246–3252 (2013).
[26]Y. Zhao, J. Qiao, Z. Yu, P. Yu, K. Xu, S. P. Lau, W. Zhou, Z. Liu, X. Wang, W. Ji, and Y. Chai, "High-electron-mobility and air-stable 2D layered $PtSe_2$ FETs," Adv. Mater. **29**, 1604240 (2017).
[27]Y.-H. Chang, W. Zhang, Y. Zhu, Y. Han, J. Pu, J.-K. Chang, W.-T. Hsu, J.-K. Huang, C.-L. Hsu, M.-H. Chiu, T. Takenobu, H. Li, C.-I. Wu, W.-H. Chang, A. T. S. Wee, and L.-J. Li, "Monolayer $MoSe_2$ grown by chemical vapor deposition for fast photodetection," ACS Nano **8**, 8582–8590 (2014).
[28]C. Lan, C. Li, Y. Yin, and Y. Liu, "Large-area synthesis of monolayer WS_2 and its ambient-sensitive photo-detecting performance," Nanoscale **7**, 5974–5980 (2015).
[29]Y. Zhao, J. Qiao, P. Yu, Z. Hu, Z. Lin, S. P. Lau, Z. Liu, W. Ji, and Y. Chai, "Extraordinarily strong interlayer interaction in 2D layered PtS_2," Adv. Mater. **28**, 2399–2407 (2016).
[30]Y. Wang, L. Li, W. Yao, S. Song, J. T. Sun, J. Pan, X. Ren, C. Li, E. Okunishi, Y. Q. Wang, E. Wang, Y. Shao, Y. Y. Zhang, H. Yang, E. F. Schwier, H. Iwasawa, K. Shimada, M. Taniguchi, Z. Cheng, S. Zhou, S. Du, S. J. Pennycook, S. T. Pantelides, and H. J. Gao, "Monolayer $PtSe_2$, a new semiconducting transition-metal-dichalcogenide, epitaxially grown by direct selenization of Pt," Nano Lett. **15**(6), 4013–4018 (2015).
[31]C. Yim, K. Lee, N. McEvoy, M. O'Brien, S. Riazimehr, N. C. Berner, C. P. Cullen, J. Kotakoski, J. C. Meyer, M. C. Lemme, and G. S. Duesberg, "High-performance hybrid electronic devices from layered $PtSe_2$ films grown at low temperature," ACS Nano **10**, 9550–9558 (2016).
[32]W. Yao, E. Wang, H. Huang, K. Deng, M. Yan, K. Zhang, T. Okuda, L. Li, Y. Wang, H. Gao, C. Liu, W. Duan, and S. Zhou, "Direct observation of spin-layer locking by local Rashba effect in monolayer semiconducting $PtSe_2$ film," Nat. Commun. **8**, 14216 (2017).
[33]G. Kresse and D. Joubert, "From ultrasoft pseudopotentials to the projector augmented-wave method," Phys. Rev. B **59**, 1758–1775 (1999).
[34]K. S. Novoselov, D. Jiang, T. J. Booth, W. Khotkevich, S. V. Morozov, and A. K. Geim, "Two-dimensional atomic crystals," Proc. Natl. Acad. Sci. U.S.A. **102**, 10451–10453 (2005).
[35]S. Grimme, J. Antony, S. Ehrlich, and H. Krieg, "A consistent and accurate *ab initio* parametrization of density functional dispersion correction (DFT-D) for the 94 elements H-Pu," J. Chem. Phys. **132**, 154104 (2010).
[36]S. Baroni, S. de Gironcoli, A. Dal Corso, and P. Giannozzi, "Phonons and related crystal properties from density-functional perturbation theory," Rev. Mod. Phys. **73**, 515–562 (2001).
[37]X. Gu and R. Yang, "Phonon transport in single-layer transition metal dichalcogenides: A first-principles study," Appl. Phys. Lett. **105**, 131903 (2014).
[38]D. Holec, M. Friak, J. Neugebauer, and P. H. Mayrhofer, "Trends in the elastic response of binary early transition metal nitrides," Phys. Rev. B **85**, 064101 (2012).
[39]Z. Huang, W. Zhang, and W. Zhang, "Computational search for two-dimensional MX_2 semiconductors with possible high electron mobility at room temperature," Materials **9**, 716–729 (2016).
[40]S. D. Guo and J. L. Wang, "Spin-orbital coupling effect on the power factor in semiconducting transition-metal dichalcogenide monolayers," Semicond. Sci. Technol. **31**, 095011 (2016).
[41]H. L. Zhuang and R. G. Hennig, "Computational search for single-layer transition-metal dichalcogenide photocatalysts," J. Phys. Chem. C **117**, 20440–20445 (2013).
[42]F. A. Rasmussen and K. S. Thygesen, "Computational 2D materials database: Electronic structure of transition-metal dichalcogenides and oxides," J. Phys. Chem. C **119**, 13169–13183 (2015).
[43]T. Olsen, S. Latini, F. Rasmussen, and K. S. Thygesen, "Simple screened hydrogen model of excitons in two-dimensional materials," Phys. Rev. Lett. **116**, 056401 (2016).
[44]H. L. Zhuang and R. G. Hennig, "Theoretical perspective of photocatalytic properties of single-layer SnS_2," Phys. Rev. B **88**, 115314 (2013).